Research Article Vol. 4, No. 3 / March 2017 / Optica 367

Three-dimensional multiple-particle tracking with nanometric precision over tunable axial ranges

Giuseppe Sancataldo,[1,2] Lorenzo Scipioni,[1,2] Tiziana Ravasenga,[1,3] Luca Lanzanò,[1] Alberto Diaspro,[1] Andrea Barberis,[3] and Martí Duocastella[1,*]

[1]Nanoscopy, Istituto Italiano di Tecnologia, Via Morego 30, 16123 Genova, Italy
[2]Dibris, Università di Genova, Via All'Opera Pia 13, Genova, Italy
[3]Neuroscience and Brain Technologies, Istituto Italiano di Tecnologia, Via Morego 30, 16123 Genova, Italy
*Corresponding author: marti.duocastella@iit.it

Received 17 January 2017; revised 19 February 2017; accepted 19 February 2017 (Doc. ID 284821); published 13 March 2017

The precise localization of nanometric objects in three dimensions is essential to identify functional diffusion mechanisms in complex systems at the cellular or molecular level. However, most optical methods can achieve high temporal resolution and high localization precision only in two dimensions or over a limited axial (z) range. Here we develop a novel wide-field detection system based on an electrically tunable lens that can track multiple individual nanoscale emitters in three dimensions over a tunable axial range with nanometric localization precision. The optical principle of the technique is based on the simultaneous acquisition of two images with an extended depth of field while encoding the z position of the emitters via a lateral shift between images. We provide a theoretical framework for this approach and demonstrate tracking of free diffusing beads and GABAA receptors in live neurons. This approach allows getting nanometric localization precision up to an axial range above 10 μm with a high numerical aperture lens—quadruple that of a typical 3D tracking system. Synchronization or complex fitting procedures are not requested here, which leads to a suitable architecture for localizing single molecules in four dimensions, namely, three dimensions in real-time.

OCIS codes: (180.0180) Microscopy; (110.0110) Imaging systems; (230.0230) Optical devices; (170.2520) Fluorescence microscopy; (100.6890) Three-dimensional image processing.

https://doi.org/10.1364/OPTICA.4.000367

1. INTRODUCTION

To unmask the dynamics of proteins, molecular complexes, vesicles, or viruses inside complex biological systems, high temporal and spatial resolution 3D single particle tracking (SPT) technologies, in which the 3D coordinates of a moving particle are retrieved from time-lapse microscopy imaging data, have been key [1]. So far, SPT has provided new insights into phenomena including virus trafficking [2], endocytosis [3], microtubule growth [4], and molecular diffusion at synapses [5]. Although various optical strategies capable of 10–100 nm localization precision in the x–y–z coordinates are now available, most of these are severely limited in axial tracking range [6,7]. Indeed, widely used 3D tracking approaches including defocus imaging [8,9] or the use of an engineered point spread function (PSF) such as the double-helix [10,11] or astigmatic [7,12] PSF, which can track particles only up to ∼3 μm in the axial direction. This is mainly caused by the spreading of light when the particle moves out of focus and the consequent decrease in signal over background. Considering that a mammalian cell—arguably the most studied system in biology—often has a thickness greater than 6 μm [13], this means that current tracking techniques cannot provide a complete characterization of nanoscale behavior within these single units. The problem is amplified when considering more complex and thicker systems, such as cell aggregates or organotypic cultures [14]. Therefore, a current challenge in 3D tracking technologies is to develop an approach that can concentrate the light detected from an emitter into a small region throughout a long axial range (>5 μm), while still maintaining the ability to recognize the z position of the particle with nanometric precision.

Efforts to extend the axial tracking range in SPT include using feedback control systems to actively maintain the emitter in focus, such as in orbital tracking [15]. While providing temporal resolutions down to 1 ms, feedback approaches are intrinsically constrained to operate with one particle at a time [16]. Importantly, real applications often require "multiple-particle tracking," namely, the simultaneous tracking of many individual particles (tens to hundreds) [17]. Alternatively, the simultaneous imaging of multiple focal planes can be applied in wide-field microscopes to successfully track particles over an axial range typically below 10 μm [9,18–21]. This method, however, can be difficult to implement in practice due to the complexity of the setup, and when more than two planes are used, may result in a significant decrease

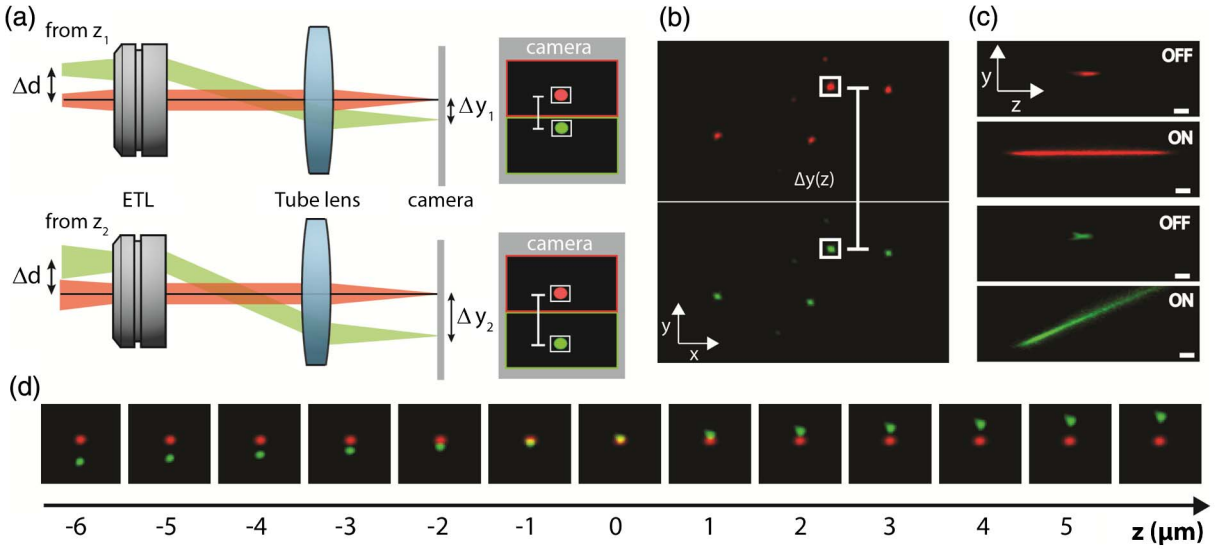

Fig. 1. Schematic of the working principle of the tracking approach. (a) Red beams show the effect of the tunable lens in a standard on-axis image formation system. For an infinity corrected system, the focal length of an ETL placed in the conjugate plane of the detection objective can be varied to compensate for any degree of divergence for rays coming from focal planes at different z positions (bottom). This enables the formation of focused images at the camera sensor for particles located at different z positions, preventing the loss of out-of-focus tracking precision. By inserting an off-axis displacement of the ETL relative to the optical axis, the same holds (green beam). However, in this case, there is an additional steering effect that depends on the value of the ETL focal length needed to bring the image into focus. This produces an encoding of the axial position into a lateral shift. (b) Snapshot of a sample of fluorescent beads acquired with the tracking system. The false colors correspond to the aligned (red) and decentered (green) channels. (c) Experimental PSF for each channel with the ETL off (standard acquisition system) and ETL on. Scale bar is 2 μm. (d) Lateral shift induced in the green channel for a single bead as a function of the axial position. Note that the red channel does not move.

in localization precision. Recent work using a tetrapod PSF has demonstrated an impressive axial tracking range [22]. In this case, advanced fitting procedures are required to retrieve the z position from such a PSF, and localization precision can be seriously degraded by aberrations in the sample that distort the shape of the PSF. More recently, 4Pi microscopy has been used for whole-cell axial range single molecule localization [23]. Despite imaging 3D structures with 10–20 nm precision, the required setup is rather complicated, with the need to use two opposing objective lenses and two deformable mirrors. Furthermore, most existing techniques lack tunability in the selection of the axial tracking range or the localization precision, which impedes tailoring these parameters to different applications. Simply put, a multi-particle tracking method with nanometer precision and (at least) whole-cell axial range that is easy to implement in a conventional wide-field microscope and provides tunable axial range according to the application does not exist.

In this paper, we present a novel optical configuration that enables tracking of particles with nanometric precision (in the lateral and axial directions) over a tunable axial range above 10 μm. A straightforward implementation, based on the acquisition of two simultaneous wide-field images of the specimen and an electrically tunable lens (ETL), is used. An ETL allows the position of the focal image plane to be changed across a large axial range much faster than the exposure time of the camera detector. Roughly speaking, an ETL allows a particle to be maintained in focus even if it is moving comparatively quickly across the axial range, an effect usually referred to as extended depth of field or EDOF [24–26] (see Supplement 1, Section 1). Thus, the first acquired image in the current approach is formed after passing through the optical axis of the ETL. Because of the EDOF effect, particles appear as bright spots across a long axial range, and the particles can be easily localized in x and y [Fig. 1(a), red beam] with a precision similar to current SPT methods. The second image uses a light pathway that is decentered with respect to the ETL optical axis. In this case, the image of the particle corresponds to a bright spot that is laterally shifted with respect to the first one (see Fig. S4 in Supplement 1). Such a shift linearly depends on the z position of the particle (see Supplement 1, Section 2). As a result, by measuring the lateral distance between the spots of the two images, we can locate the z position of the emitters [Fig. 1(a), green beam]. Importantly, by tuning the system parameters (off-axis displacement of the ETL, etc.) it is possible to select the tracking range or axial localization precision, rendering this approach electronically tunable. We characterized the technique in detail and demonstrate its feasibility by tracking diffusion beads in water and inhibitory neurotransmitter receptors in the soma of live neurons.

2. RESULTS AND DISCUSSION

Initially, we experimentally validated the capability of the 3D tracking system to generate an EDOF as well as to retrieve the axial information of single particles. To this end, we modified a commercial inverted microscope to split the detection arm into two pathways and accommodate the ETL (Fig. S5, Supplement 1). We used simple optical elements to achieve this, including a relay system with unit magnification, a beam splitter, and different mirrors that allow the independent alignment of each light path. Thus, each pathway can be directed to the ETL at different distances from the lens optical axis. We used additional mirrors placed after the ETL to direct the two pathways into two separate regions of a single electron multiplying CCD (EMCCD). Hereafter, we refer to each of the two regions as a

channel. Therefore, all the information required for 3D tracking was gathered in a single frame; an image to determine the x–z coordinates of the emitter (aligned with respect to the ETL optical axis), and a second image to obtain the emitter z position (decentered with respect to the ETL optical axis). A typical snapshot of 500 nm fluorescent beads attached to a coverslip with the ETL on (driven with a triangular signal at 10 Hz) is presented in Fig. 1(b). The two channels were false colored: red and green correspond to the aligned and decentered channels, respectively. Importantly, the separation along the y axis between the two images formed for each individual bead contains information on the bead relative axial position [$\Delta y(z)$ in Fig. 1(b)]. Similar approaches have been reported to encode the axial position of a single particle by using mirrors [27], a wedge prism [28], or stereo illumination [29], but none of these could track a particle beyond a 1 μm axial range.

The experimentally reconstructed PSF of our system obtained using 100 nm beads [Fig. 1(c)], provides an intuitive picture of the ETL-based tracking approach implemented here. Compared to the native response of the microscope (ETL off), the ETL produces, for both red and green channels, an elongated PSF over a range of about 12 μm (ETL on). Thus, any particle located within this EDOF appears in the detector as two well-defined spots (one red, one green) and the corresponding x–y coordinates can be determined with high localization precision. Notably, the PSF of the green channel is not only elongated, but also displays a significant tilting along the y–z plane. This implies that the position of the green spot in the detector shifts laterally along the y axis depending on the particle axial position. Such an effect can be better appreciated in Fig. 1(d). In this case, the two channels were superimposed. As expected, when a single particle is axially translated within the EDOF, the detected red spot does not move or change size, and thus the x–y coordinates of the particle can be easily determined. In contrast, the detected green spot shifts along the y direction. Therefore, by measuring the y separation between the red and green spots one can unequivocally determine the relative z position of a particle.

To quantify the localization precision of this 3D tracking approach, a series of images of 500 nm fluorescent beads attached to a cover slip at different axial positions was acquired. We used two different configurations, with the green channel decentered by a different amount Δd. In both cases, 50 images were acquired at each axial position in steps of 0.5 μm. This experiment also served as the calibration step necessary to determine the relationship between lateral displacement and axial position. A custom fit-free algorithm based on the fast Fourier transform (FFT) was used to quantify the distance Δy between the images of each particle in the two channels (see Supplement 1, Section 6). Note that a normal fitting algorithm could be used as well, but a FFT fitting-free algorithm has advantages in terms of processing time, and could lead to real-time tracking. The plot of the distance Δy for a single bead as a function of its axial position for the two configurations is shown in Fig. 2(a) (small decentering, $\Delta d =$ 800 μm in blue, large decentering, $\Delta d = 1500$ μm in red). Δy in the two experimental settings changes linearly with the z position within axial ranges of about 12 μm and 2 μm, respectively. This is in agreement with a simple model based on geometrical optics that predicts the relationship between these parameters given by (see Supplement 1, Section 2)

$$\Delta y = Cz = \frac{f_t \Delta d}{M_R^2 f_o^2} z, \tag{1}$$

where C is a proportionality constant, M is the magnification factor of the relay system, and f_t and f_o the focal lengths of the tube lens and objective, respectively. In the current conditions, the parameter constant C results in 2.7 pixel/μm for the small decentering and 5.1 pixels/μm for the large decentering. Considering the effective pixel size to be 160 nm, the corresponding C values are 0.43 and 0.82. Figure 2(b) shows, for the two analyzed conditions, the x–y–z position of a single bead along the axial range of the calibration sequence. The calculation of the standard deviation from these plots enables the localization precision of the approach to be determined. In particular, for a mean

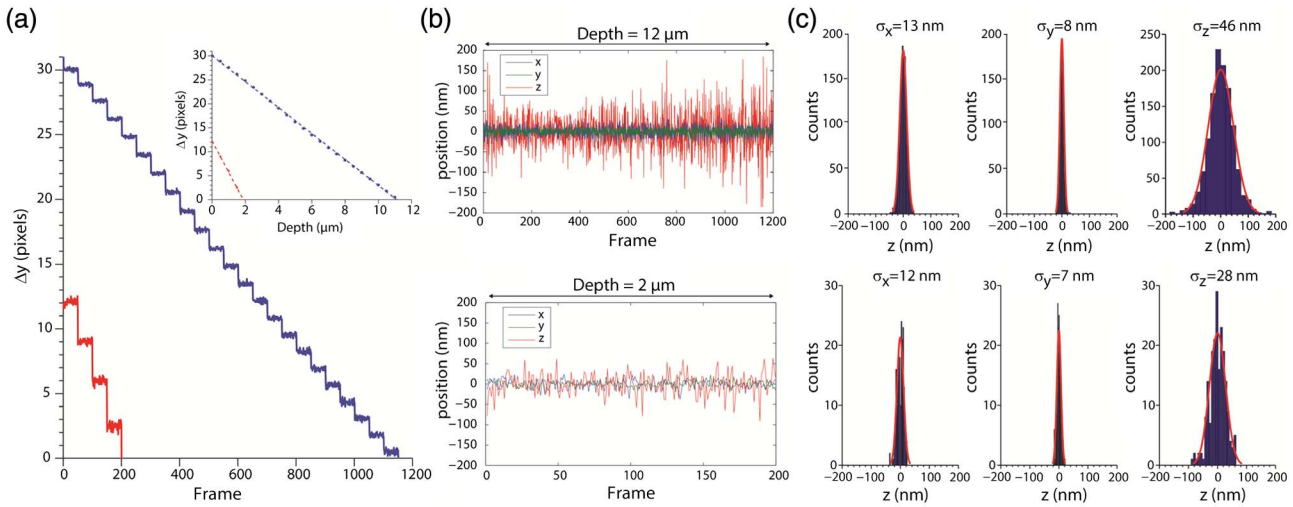

Fig. 2. Characterization of the localization precision of the 3D tracking technique. (a) Lateral separation between the two channels (Δy), in pixels, for a 500 nm bead attached to a glass coverslip and translated in steps of 0.5 μm every 50 acquisitions. The experiment was repeated for two different settings: a value of C corresponding to 2.7 px/μm (blue line) for a total axial range of 12 μm and to 5.1 px/μm (red line) for an axial range of 2 μm. The inset shows the linear dependence of Δy as a function of the axial position for each case. (b) Plot of the x–y–z position of the tracked bead in (a) along the entire axial range for the two studied configurations. The values have been calculated relative to the average position in each axial plane. (c) Localization precision along the three directions of space extracted from (b).

number of ~5500 signal photons and ~21 background photons per pixel, the lateral localization ($\sqrt{\sigma_x^2 + \sigma_y^2}$) was about 15 nm for both experimental settings, while the axial localization precision was 46 and 28 nm for the small and the large decentering conditions, respectively [Fig. 2(c)].

The achieved results demonstrate the unique tunability of the system, capable of performing nanometric precision particle tracking over user-selectable micrometer axial ranges. However, the values reported here for localization precision are strongly influenced by the large parameter space (emitters/fluorophores per particle, quantum yield emitter, illumination source, camera, objective, etc.) that comes with any SPT approach. Therefore, it is difficult to directly compare the current values with those reported in the literature using other tracking methods. Instead, the square root of the Cramer–Rao lower bound ($CRLB^{1/2}$) provides the best localization precision theoretically possible with a particular tracking approach, and has become the tool of choice to qualitatively evaluate the performance of photon-limited 3D-SPT methods. Compared to single plane or multiplane SPT, the calculation of the $CRLB^{1/2}$ for our method reveals a uniform localization precision in the three directions of space within the EDOF (see Supplement 1, Section 3). Because the axial position of a particle is obtained from its distance in the y axis across the two channels, the localization precision in the z direction (σ_z) depends on the localization precision in the y axis (σ_y) and the proportionality constant C [Eq. (1)] as

$$\sigma_z = \frac{\sqrt{2}}{C}\sigma_y. \tag{2}$$

Consequently, provided $C > \sqrt{2}$, it is possible to obtain a better localization precision along the z direction than along the x or y axis. Indeed, as we have experimentally demonstrated, the selection of the factor C by tuning the system parameters enables the selection of the localization precision along the z axis.

Despite the theoretical predictions based on the CRLB, there are several experimental factors that can contribute to the loss of tracking precision uniformity (across the axial range) or that can limit the total tracking axial range of our approach. These limiting factors are mainly related to the current technology of the ETL used in our optical system. For example, the finite geometrical aperture of the lens imposes a maximum achievable off-axis decentering (and thus constant C) that limits the tunability of the axial localization precision. Indeed, if the physical aperture of the ETL partially blocks the off-center pathway, the effective numerical aperture of the objective lens will decrease, which will cause a loss in tracking precision. As a second example, the scanning behavior of the lens can introduce aberrations when particles are tracked in planes that are far from the native one of the imaging system [30], which can degrade tracking precision at these positions. These factors, however, could be compensated for by using other new and upcoming types of tunable lenses with large apertures and incorporated aberration compensation capabilities [31]. An additional aspect of our approach impacts the accuracy of localization. The potential refractive index mismatch when tracking objects in water or other aqueous solutions can result in aberrations that degrade localization accuracy. However, at current conditions accuracy is preserved for at least a range of 20 μm (see Fig. S6 in Supplement 1). Furthermore, when large numbers of particles are tracked, at a given time, some PSFs may be coaligned along the y axis. This situation would prevent appropriate determination of the z position of the corresponding particles. Naturally, information of past and future localizations of the particle may help resolve the ambiguity and restore the appropriate trajectory. Tracking high numbers of particles is inherently problematic in SPT due to overlap of the PSFs of closely spaced emitters [32]. However, compared to engineered PSFs [22] or defocus-based methods [9], our tracking approach maintains a highly lateral, confined PSF along the EDOF, helping mitigate these effects.

We validated our method with a simple experiment, tracking free-diffusing microspheres in an aqueous solution. The 3D trajectory of a 500 nm fluorescent bead in water at room temperature was reconstructed, for a total time of 100 s and at 10 fps [Fig. 3(a)]. A time-lapse movie of the two acquired channels corresponding to the same bead is reconstructed in Visualization 1. The channels have been overlapped as in Fig. 1(d) for visualization. From this data, it is possible to extract quantitative information from the bead dynamics. In particular, the mean square displacement normalized to time and to the number of spatial dimensions (MSD) can be directly calculated [Fig. 3(b)]. A simple linear fitting can then be used to calculate the diffusion coefficient (D) of the bead [33], which results in $D = 0.90 \pm 0.16\ \mu m^2/s$. This value agrees well with that previously reported for beads of the same size in an aqueous media ($D = 0.875\ \mu m^2/s$), confirming the validity of our technique [34].

We next attempted 3D tracking of proteins diffusing on the membrane surface of living neurons. In particular, we focused on neurotransmitter receptors, transmembrane proteins crucial for information transfer between neurons. Neurotransmitter receptors rapidly diffuse in the neuronal membrane, and the dynamic exchange between different neuronal compartments is responsible for the coding and processing of information in neuronal

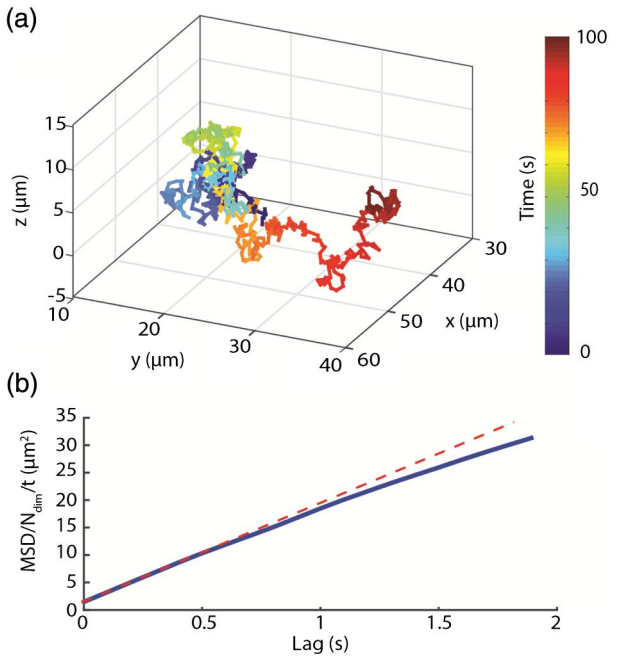

Fig. 3. Measurement of the 3D free-diffusion coefficient of microspheres in water. (a) 3D trajectory of single fluorescent bead (500 nm size) tracked in water at room temperature. The 3D position of the fluorescent particle was measured every 0.1 s for 100 s. (b) Representative MSD plot for the freely diffusing particle shown in (a).

networks [35,36]. To date, fast diffusion of receptors has been determined by the analysis of receptor 2D trajectories, mainly due to the limitations of technology in providing information on receptor displacement along the z-axis. For this reason, the study of receptor mobility has been restricted to "flat" (few hundred nanometers) sub-regions of neurons (dendrites and axons) grown in planar substrate. 3D receptor tracking has never been attempted on the soma of cultured neurons (which approximates a spherical cap of a few micrometers in the z axis) or in neurons embedded in a 3D texture, such as in brain tissue. We tested the capability of our system to perform fast 3D tracking of inhibitory receptors (GABAA receptors) on the soma of cultured hippocampal neurons (Fig. 4 and Visualization 2). To this end, we coupled receptors to quantum dots (QDs) via a primary antibody and imaged QD diffusion on the neuronal somatic region. Indeed, an individual GABAA receptor can be visualized diffusing on the soma surface (Fig. 4). Interestingly, the GABAA receptor displays complex diffusion patterns, including free diffusion and more confined mobility (at 25–30 and 0 s–5 s, respectively, in Fig. 4(b). Confined lateral mobility likely reflects transient GABAA receptor binding to anchoring proteins and/or the molecular crowding at specific neuronal molecular subdomains [36]. In this experiment, the localization precision for ~500 signal photons and ~22 background photons per pixel, measured as in Figure 2(a), was 30 nm and 60 nm in the lateral and axial direction, respectively, (with $C = 2.7$ pixels/μm). These data reveal that this optical system is suitable for 3D fast tracking of single molecules in living biological samples.

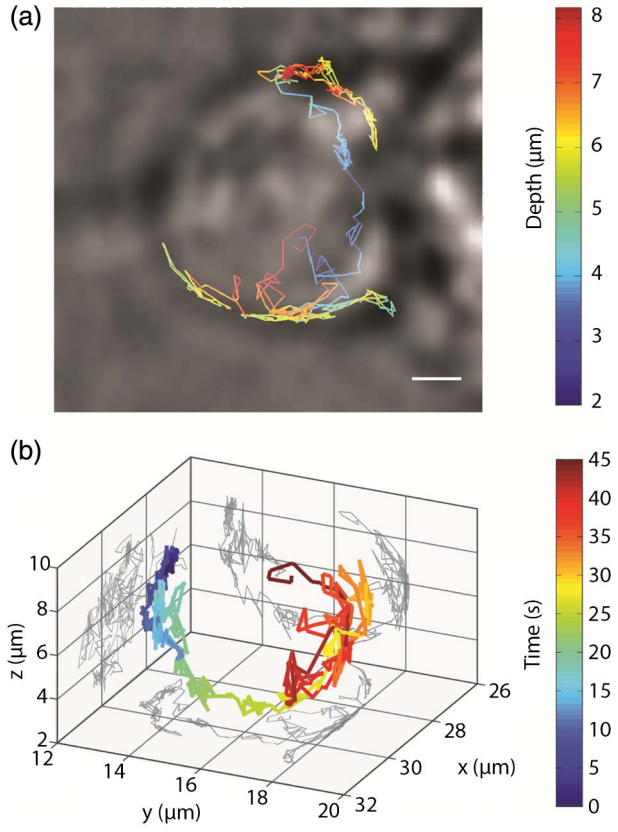

Fig. 4. Diffusion of GABAA receptors in the membrane of living neurons. (a) Representative time-color-coded trajectory of an individual α1-containing GABAA receptor diffusing on a soma of a cultured hippocampal neuron. The trajectory tracking the QD fluorescence has been superimposed on the neuronal soma image acquired with transmitted light microscopy. Scale bar is 2 μm. (b) Same receptor trajectory shown in (a) rendered in three dimensions and shown on a time-coded scale. In ~45 s the receptor explores a considerable portion of the somatic region spanning ~4–6 μm in both the x–y and z axes.

3. CONCLUSIONS

In summary, an ETL can be used to track multiple particles with nanometric localization precision over micrometric and user-controllable axial ranges. The proposed solution addresses two main problems in existing 3D tracking approaches: the concentration of the detected light from emitters into a small region over a wide axial range, and the efficient encoding of the z position of the emitter. Because the axial localization precision and axial range can be chosen, this system can accommodate the demands of a particular biological problem. The setup is based on a simple optical modification of a commercial wide-field system, and can be integrated into a compact modular device. The possibility of using fitting-free algorithms facilitates the use of short temporal windows for high-speed 3D-tracking. We anticipate that the same optical system and detection/localization algorithm can be easily applied to single molecule localization methods, offering a powerful tool for real-time, super-resolution imaging over large volumes.

4. METHODS

A. Optical Setup

The 3D-tracking approach was implemented by adapting a wide-field inverted microscope (Nikon Ti) with an infinity-corrected oil-immersion objective (Nikon 100 × Plan Apo VC 100 × /1.4 oil DIC N2), a high-intensity lamp, a piezoelectric stage (Mad City Lab) for z translation of the sample, and a single EMCCD camera (DU897DCS-BV, Andor Technology; 16 μm × 16 μm pixel size; Fig. S5 in Supplement 1). The detection arm was split into two pathways as well as to accommodate the ETL (Optotune, EL-10-30) at a conjugate plane of the back focal plane of the objective. To this end, we placed a relay system with unit magnification ($f = 200$ mm), a 50:50 beam splitter and a set of four mirrors each to adjust the alignment of each path independently. Thus, each path could be directed to the varifocal lens at different distances from the ETL optical axis. Two additional sets of four mirrors placed after the ETL were used to focus each pathway into two separate regions of the EMCCD. In all experiments, camera exposure time was 100 ms. A dichroic mirror was used to select an excitation wavelength of 488 nm and collect fluorescence at 655 nm.

B. Bead Sample Preparation

Immobilized beads: fluorescent microspheres (TetraSpeck 100 or 500 nm, fluorescent blue, green, orange, and dark; ThermoFisher, U.S.) were diluted in Milli-Q water with a dilution factor of 10^4. A drop of diluted beads was attached to the coverslip using poly-L-lysine (Sigma Aldrich) and then mounted on a microscope slide using ProLong Gold Antifade (ThermoFisher) as a mounting medium.

Diffusing beads: suspensions of fluorescent microspheres (TetraSpeck 500 nm, fluorescent blue, green, orange, and dark; ThermoFisher) were diluted in Milli-Q water with a dilution

factor of 10^3. A volume of 200 μl in a Nunc chamber (ThermoFisher) was used for diffusion studies.

C. Biological Sample Preparation

All experiments were carried out in accordance with the guidelines established by the European Communities Council (Directive 2010/63/EU of 22 September 2010), were permitted by the Italian Ministry of Health, and followed the rules approved by the Italian Institute of Technology. All animal surgeries were done in agreement with the Italian Ministry of Health Regulation and Authorization and were approved by the Italian Institute of Technology. Neurons were plated at a density of 90×10^3 cells/cm^2 on poly-D-lysine pre-coated coverslips and kept in serum-free Neurobasal-A medium (Invitrogen, Italy) supplemented with 1% Glutamax (Invitrogen), 2% B-27 (Invitrogen) and 5 mg/ml gentamycin at 37°C in 5% CO_2. All experiments were performed at 16–18 days *in vitro*. QD staining of surface GABAA receptors was performed according to previously described protocols [37]. Briefly, anti-α1 subunit antibody (against an extracellular epitope) from Alomone, Israel (AGA-001) was premixed with anti-rabbit QD 655 (Invitrogen) for 30 min in the presence of casein (Vectorlab, Italy) to prevent non-specific binding. Neurons were incubated with the diluted antibody–QD premix for 2 min at room temperature to obtain a final QD concentration of ~0.1 nM. The highly diluted QD labeling resulted in <5 QDs per field of view, so that individual QD receptor complexes did not overlap the trajectories of neighboring QD–receptor complexes. The absence of QD labeling when the primary antibody was omitted from the QD–antibody premix in control experiments confirmed antibody specificity (data not shown). During the imaging experiments, cells were bathed in an extracellular solution containing 145 mM NaCl, 2 mM KCl, 1 mM $CaCl_2$, 2 mM $MgCl_2$, 10 mM glucose, and 10 mM HEPES, pH 7.4, and were kept at 32°C. Imaging was performed with a back-illuminated EMCCD camera (Andor Ixon DU–897E–CS0BV) with an exposure time of 100 ms. A triangular signal with a frequency of 10 Hz was applied to the ETL using an Optotune USB lens driver.

Funding. Compagnia di San Paolo (SIME 2015-0682).

Acknowledgment. The authors thanks Giuseppe Vicidomini for valuable discussions in preparing this manuscript.

See Supplement 1 for supporting content.

REFERENCES

1. A. Dupont and D. C. Lamb, "Nanoscale three-dimensional single particle tracking," Nanoscale **3**, 4532–4541 (2011).
2. B. Brandenburg and X. Zhuang, "Virus trafficking-learning from single-virus tracking," Nat. Rev. Microbiol. **5**, 197–208 (2007).
3. H. Jin, D. A. Heller, and M. S. Strano, "Single-particle tracking of endocytosis and exocytosis of single-walled carbon nanotubes in NIH-3T3 cells," Nano Lett. **8**, 1577–1585 (2008).
4. I. Smal, K. Draegestein, N. Galjart, W. Niessen, and E. Meijering, "Particle filtering for multiple object tracking in dynamic fluorescence microscopy images: application to microtubule growth analysis," IEEE Trans. Med. Imaging **27**, 789–804 (2008).
5. E. M. Petrini, T. Ravasenga, T. J. Hausrat, G. Iurilli, U. Olcese, V. Racine, J.-B. Sibarita, T. C. Jacob, S. J. Moss, F. Benfenati, P. Medini, M. Kneussel, and A. Barberis, "Synaptic recruitment of gephyrin regulates surface GABAA receptor dynamics for the expression of inhibitory LTP," Nat. Commun. **5**, 3921 (2014).
6. H. Deschout, F. Cella Zanacchi, M. Mlodzianoski, A. Diaspro, J. Bewersdorf, S. T. Hess, and K. Braeckmans, "Precisely and accurately localizing single emitters in fluorescence microscopy," Nat. Methods **11**, 253–266 (2014).
7. M. J. Mlodzianoski, M. F. Juette, G. L. Beane, and J. Bewersdorf, "Experimental characterization of 3D localization techniques for particle-tracking and super-resolution microscopy," Opt. Express **17**, 8264–8277 (2009).
8. M. Speidel, A. Jonás, and E.-L. Florin, "Three-dimensional tracking of fluorescent nanoparticles with subnanometer precision by use of off-focus imaging," Opt. Lett. **28**, 69–71 (2003).
9. E. Toprak, H. Balci, B. H. Blehm, and P. R. Selvin, "Three-dimensional particle tracking via bifocal imaging," Nano Lett. **7**, 2043–2045 (2007).
10. M. A. Thompson, M. D. Lew, M. Badieirostami, and W. E. Moerner, "Localizing and tracking single nanoscale emitters in three dimensions with high spatiotemporal resolution using a double-helix point spread function," Nano Lett. **10**, 211–218 (2010).
11. S. R. P. Pavani, M. A. Thompson, J. S. Biteen, S. J. Lord, N. Liu, R. J. Twieg, R. Piestun, and W. E. Moerner, "Three-dimensional, single-molecule fluorescence imaging beyond the diffraction limit by using a double-helix point spread function," Proc. Natl. Acad. Sci. USA **106**, 2995–2999 (2009).
12. B. Huang, W. Wang, M. Bates, and X. Zhuang, "Three-dimensional super-resolution imaging by stochastic optical reconstruction microscopy," Science **319**, 810–813 (2008).
13. J. L. Gregg, K. M. McGuire, D. C. Focht, and M. A. Model, "Measurement of the thickness and volume of adherent cells using transmission-through-dye microscopy," Pflügers Arch. **460**, 1097–1104 (2010).
14. B. Biermann, S. Sokoll, J. Klueva, M. Missler, J. S. Wiegert, J.-B. Sibarita, and M. Heine, "Imaging of molecular surface dynamics in brain slices using single-particle tracking," Nat. Commun. **5**, 3024 (2014).
15. L. Lanzano and E. Gratton, "Orbital single particle tracking on a commercial confocal microscope using piezoelectric stage feedback," Methods Appl. Flouresc. **1**, 024010 (2014).
16. M. F. Juette and J. Bewersdorf, "Three-dimensional tracking of single fluorescent particles with submillisecond temporal resolution," Nano Lett. **10**, 4657–4663 (2010).
17. Y. Kalaidzidis, "Multiple objects tracking in fluorescence microscopy," J. Math. Biol. **58**, 57–80 (2009).
18. S. Abrahamsson, J. Chen, B. Hajj, S. Stallinga, A. Y. Katsov, J. Wisniewski, G. Mizuguchi, P. Soule, F. Mueller, C. Dugast Darzacq, X. Darzacq, C. Wu, C. I. Bargmann, D. A. Agard, M. Dahan, and M. G. L. Gustafsson, "Fast multicolor 3D imaging using aberration-corrected multifocus microscopy," Nat. Methods **10**, 60–63 (2013).
19. S. Ram, P. Prabhat, J. Chao, E. S. Ward, and R. J. Ober, "High accuracy 3D quantum dot tracking with multifocal plane microscopy for the study of fast intracellular dynamics in live cells," Biophys. J. **95**, 6025–6043 (2008).
20. M. Duocastella, C. Theriault, and C. B. Arnold, "Three-dimensional particle tracking via tunable color- encoded multiplexing," Opt. Lett. **41**, 863–864 (2016).
21. H. Li, D. Chen, G. Xu, B. Yu, and H. Niu, "Three dimensional multi-molecule tracking in thick samples with extended depth-of-field," Opt. Express **23**, 787–794 (2015).
22. Y. Shechtman, L. E. Weiss, A. S. Backer, S. J. Sahl, and W. E. Moerner, "Precise 3D scan-free multiple-particle tracking over large axial ranges with Tetrapod point spread functions," Nano Lett. **15**, 4194–4199 (2015).
23. F. Huang, G. Sirinakis, E. S. Allgeyer, L. K. Schroeder, W. C. Duim, E. B. Kromann, T. Phan, F. E. Rivera-Molina, J. R. Myers, I. Irnov, M. Lessard, Y. Zhang, M. A. Handel, C. Jacobs-Wagner, C. P. Lusk, J. E. Rothman, D. Toomre, M. J. Booth, and J. Bewersdorf, "Ultra-high resolution 3D imaging of whole cells," Cell **166**, 1028–1040 (2016).
24. S. Liu and H. Hua, "Extended depth-of-field microscopic imaging with a variable focus microscope objective," Opt. Express **19**, 353–362 (2011).
25. M. Duocastella and C. B. Arnold, "Enhanced depth of field laser processing using an ultra-high-speed axial scanner," Appl. Phys. Lett. **102**, 061113 (2013).
26. M. Duocastella, G. Vicidomini, and A. Diaspro, "Simultaneous multiplane confocal microscopy using acoustic tunable lenses," Opt. Express **22**, 19293–19301 (2014).

27. Y. Sun, J. D. McKenna, J. M. Murray, E. M. Ostap, and Y. E. Goldman, "Parallax: high accuracy three-dimensional single molecule tracking using split images," Nano Lett. **9**, 2676–2682 (2009).
28. J. Yajima, K. Mizutani, and T. Nishizaka, "A torque component present in mitotic kinesin Eg5 revealed by three-dimensional tracking," Nat. Struct. Mol. Biol. **15**, 1119–1121 (2008).
29. R. Bowman, G. Gibson, and M. Padgett, "Particle tracking stereomicroscopy in optical tweezers: control of trap shape," Opt. Express **18**, 11785–11790 (2010).
30. M. Martinez-Corral, P.-Y. Hsieh, A. Doblas, E. Sanchez-Ortiga, G. Saavedra, and Y.-P. Huang, "Fast axial-scanning widefield microscopy with constant magnification and resolution," J. Display Technol. **11**, 913–920 (2015).
31. S. Bonora, D. Coburn, U. Bortolozzo, C. Dainty, and S. Residori, "High resolution wavefront correction with photocontrolled deformable mirror," Opt. Express **20**, 5178–5188 (2012).
32. E. Meijering, I. Smal, and G. Danuser, "Tracking in molecular bioimaging," IEEE Signal Process. Mag. **23**(3), 46–53 (2006).
33. X. Michalet, "Mean square displacement analysis of single-particle trajectories with localization error: Brownian motion in an isotropic medium," Phys. Rev. E **82**, 041914 (2010).
34. R. Dzakpasu and D. Axelrod, "Dynamic light scattering microscopy. A novel optical technique to image submicroscopic motions. II: Experimental applications," Biophys. J. **87**, 1288–1297 (2004).
35. D. Choquet and A. Triller, "The dynamic synapse," Neuron **80**, 691–703 (2013).
36. L. Sabine and A. Triller, "Neurotransmitter dynamics," in *The Dynamic Synapse: Molecular Methods in Ionotropic Receptor Biology*, J. T. Kittler and S. J. Moss, eds. (CRC Press/Taylor & Francis, 2006).
37. E. M. Petrini, J. Lu, L. Cognet, B. Lounis, M. D. Ehlers, and D. Choquet, "Endocytic trafficking and recycling maintain a pool of mobile surface AMPA receptors required for synaptic potentiation," Neuron **63**, 92–105 (2009).